WPEDU-PR(18) 20506

S Buller et al.

Effects of flux-surface impurity density variation on collisional transport in stellarators

Preprint of Paper to be submitted for publication in
Journal of Plasma Physics

This work has been carried out within the framework of the EUROfusion Consortium and has received funding from the Euratom research and training programme 2014-2018 under grant agreement No 633053. The views and opinions expressed herein do not necessarily reflect those of the European Commission.

Effects of flux-surface impurity density variation on collisional transport in stellarators

S. Buller[1]†, H.M. Smith[2], P. Helander[2], A. Mollén[2], S.L. Newton[3], I. Pusztai[1]

[1]Department of Physics, Chalmers University of Technology, SE-41296 Göteborg, Sweden
[2]Max-Planck-Institut für Plasmaphysik, 17491 Greifswald, Germany
[3]CCFE, Culham Science Centre, Abingdon, Oxon OX14 3DB, UK

(Received xx; revised xx; accepted xx)

High-Z impurities in magnetic confinement devices are prone to develop density variations on the flux-surface, which can significantly affect their transport. In this paper, we generalize earlier analytic stellarator calculations of the neoclassical radial impurity flux in the mixed-collisionality regime (collisional impurity and low-collisionality bulk ions) to include the effect of such flux-surface variations. We find that only in the homogeneous density case is the transport of highly collisional impurities (in the Pfirsch-Schlüter regime) independent of the radial electric field. We study these effects for a Wendelstein 7-X (W7-X) vacuum field, with simple analytic models for the potential perturbation, under the assumption that the impurity density is given by a Boltzmann response to a perturbed potential. In the W7-X case studied, we find that larger amplitude potential perturbations cause the radial electric field to dominate the transport of the impurities. In addition, we find that classical impurity transport can be larger than the neoclassical transport in W7-X.

1. Introduction

At fusion-relevant temperatures, heavy impurities in high ionisation states, "high-Z impurities", emit a significant amount of radiation, and even a tiny fraction of impurity ions radiate enough power to seriously challenge the power balance in a reactor. High-Z impurities thus cannot be allowed to accumulate in the center of a magnetic-confinement fusion reactor.

In tokamaks, impurities are expelled from the core of the reactor by neoclassical transport if their temperature gradient is sufficiently large – a situation known as *temperature screening*. In stellarators, the outlook has been more pessimistic, as the radial transport is not independent of the radial electric field, and an inward pointing electric field is predicted for a stellarator reactor, which would transport impurities inwards (Hirsch *et al.* 2008).

Recent analytical results on neoclassical stellarator impurity transport have however shown that when the plasma is in a mixed-collisionality regime – where the bulk ions are at low collisionality ($1/\nu$ or $\sqrt{\nu}$ regimes) and the impurity ions are collisional – the radial impurity flux becomes independent of the electric field, which allows temperature screening to be effective in stellarators (Newton *et al.* 2017; Helander *et al.* 2017). This is due to a cancellation between the flux driven by impurity parallel flow and

† Email address for correspondence: bstefan@chalmers.se

the ion thermodynamic forces. Similar cancellation is also found in the regimes where both ions and impurities are collisional (Braun & Helander 2010), although in this case, thermodiffusion is usually inward unless the effective charge is very small, so no temperature screening occurs (Rutherford 1974).

However, high-Z impurities are also sensitive to flux-surface variations in the electrostatic potential, in response to which they can develop density variations on flux-surfaces. Such variations can have large effects on the neoclassical transport, as has been demonstrated analytically (Angioni & Helander 2014; Calvo *et al.* 2018) and numerically (Angioni *et al.* 2014; García-Regaña *et al.* 2017; Mollén *et al.* 2018) for tokamaks and stellarators. For the effects on turbulent transport in tokamaks, see for example Mollén *et al.* (2012, 2014); Angioni *et al.* (2014).

In this work, we generalize the analytical calculation in (Newton *et al.* 2017) to account for flux-surface variation of the impurity density in stellarators, using a fluid description for the impurities and solving for the ion distribution function in the $1/\nu$ regime. Our expression for the impurity flux agrees with that in Calvo *et al.* (2018), where the same problem is treated fully kinetically. Like Calvo *et al.* (2018), we find that the effect of the radial electric field can be large when the amplitude of the flux-surface variation is large. In addition, we find that classical transport can be dominant compared to the neoclassical transport for collisional impurities in certain stellarator geometries.

The remainder of this paper is organised as follows: in Sec. 2, we present the equations describing the impurities, and relate the friction force acting on the impurities to their flux-surface density variations and the resulting radial flux. In Sec. 3, we introduce the ion-impurity collision operator and obtain an explicit expression for the ion-impurity friction force. In Sec. 4, we consider simplifying limits of the equations presented in the previous sections, and derive expressions for transport coefficients in those limits. Sec. 5 treats the classical transport, and shows why it is important in Wendelstein 7-X. Finally, in Sec. 6, we apply our results to study a test-case based on a Wendelstein 7-X vacuum field.

2. Impurity equations

In this section, we present equations to model the impurities, starting from momentum balance and ending with expressions for calculating the flux along the magnetic field and across the flux-surface.

The impurities are assumed to be collisional enough to be in the Pfirsh-Schlüter regime and thus have a Maxwellian velocity distribution, with the density not necessarily constant on flux-surfaces. For such a species in steady-state, the momentum equation is

$$\nabla p_z = Zen_z\boldsymbol{E} + Ze\boldsymbol{\Gamma}_z \times \boldsymbol{B} + \boldsymbol{R}_z \tag{2.1}$$

where the z species subscript refers to the impurities, Z is the impurity charge-number, e the proton charge, p_z the impurity pressure, n_z the impurity density, $\boldsymbol{\Gamma}_z$ the impurity particle flux, $\boldsymbol{B}$ the magnetic field, $\boldsymbol{E}$ the electric field, and $\boldsymbol{R}_z$ is the friction force acting on the impurities. By projecting (2.1) onto the magnetic field direction $\boldsymbol{b} = \boldsymbol{B}/B$, with $B = |\boldsymbol{B}|$, we obtain

$$\nabla_\parallel p_z = Zen_z E_\parallel + R_{z\parallel}. \tag{2.2}$$

From (2.2), we see that pressure (and thus density) variation along the field-line is set up by forces associated with the parallel electric field and friction – both of which increase with the impurity charge number. The friction force can be calculated using kinetic

information of all other species, as

$$\boldsymbol{R}_z = m_z \sum_a \int \mathrm{d}^3 v \, \boldsymbol{v} C[f_z, f_a], \tag{2.3}$$

where f_a is the distribution function of a species "a". We will restrict ourselves to the case where only collisions between a bulk ion species i and the impurities matter: the electron contribution to the friction force can be neglected as small in the electron-ion mass ratio.

In order to simplify the kinetic calculations required to determine f_i, we will assume that $Z \gg 1$, so that the effects that lead to pressure variation on the flux-surface are small for the bulk ions. In the $Z \gg 1$ limit, the ions and impurities will have undergone temperature equilibration if (Helander 1998)

$$\frac{\rho_* \hat{\nu}_{ii}}{Z} \ll 1, \tag{2.4}$$

where $\rho_* = \rho_i / L$, with L the profile length-scale and $\rho_i = v_{Ti} m_i / eB$ the ion thermal gyroradius, with m_i the ion mass and $v_{Ti} = \sqrt{2T_i/m_i}$ the ion thermal speed; $\hat{\nu}_{ii} = n_i e^4 \ln \Lambda \, L_\parallel / (T_i^2 \epsilon_0^2 12\pi^{3/2})$ is the ion collisionality where $L_\parallel$ is the length-scale of the n_z- and Φ-variations parallel to $\boldsymbol{B}$; ϵ_0 the vacuum permittivity and $\ln \Lambda$ the Coulomb-logarithm. Equation 2.4 is practically always satisfied in a magnetized plasma, so we will assume that $T_z = T_i$ is a flux-function, and (2.2) thus becomes an equation for the flux-surface variation of n_z.

Furthermore, if $\Delta \equiv Z^2 \rho_* \hat{\nu}_{ii} \ll 1$, as in the conventional drift-kinetic ordering, the friction force in (2.2) becomes smaller than the other terms (Helander 1998). To zeroth order in Δ, the density in (2.2) is then given by a Boltzmann response to Φ

$$n_z = N_z \mathrm{e}^{-Ze\Phi/T_z}, \qquad (\Delta \ll 1) \tag{2.5}$$

where N_z is a flux-function. If the density variation of all species is given by (2.5), quasi-neutrality forces the density to also be a flux-function. For significant density variation to arise on a flux-surface, one of these assumptions thus has to be violated; several different mechanisms have been considered in the literature:

In Helander (1998), $\Delta = \mathcal{O}(1)$, so the impurities themselves set up their own flux-surface variation to balance the flux-surface variation of the friction force and electric field. This was generalized in Fülöp & Helander (1999) to include centrifugal forces.

Heating can introduce a fast particle population, which may not have a density variation according to (2.5) and thus leads to an electric field tangential to the flux surface, which the impurity density in (2.2) responds to. Such effects were considered in Kazakov *et al.* (2012) and Angioni & Helander (2014), and are often more important than the variations set up by the impurities themselves.

Furthermore, in stellarators, helically trapped particles drifting due to the radial electric field can cause an in-out density asymmetry that, in turn, causes an electric field (García-Regaña *et al.* 2017). This electric field then affects the impurities. This mechanism has been investigated numerically in García-Regaña *et al.* (2017), and was found to significantly affect the transport in the Large Helical Device (LHD) and TJ-II stellarators, but does not appear to have a major effect in Wendelstein 7-X (W7-X) due to the neoclassical optimization reducing the radial extent of such helically trapped orbits.

To be able to treat all of these scenarios, we will allow Φ and Δ to be arbitrary, as long as the tangential variation in Φ (which we denote by $\tilde{\Phi}$), is of magnitude $e\tilde{\Phi}/T_i \sim Z^{-1}$

so that its effect can be neglected for the bulk ions. In Sec. 4, we will consider the case when $\Delta \ll 1$ with Φ set by fast particles.

2.1. *Radial impurity flux*

Regardless of the mechanisms that determine the spatial variation of n_z, we can calculate the perpendicular flux of the Maxwellian impurities by applying $\boldsymbol{B}\times$ to (2.1), resulting in

$$\boldsymbol{B}\times\nabla p_z = \boldsymbol{B}\times Zen_z\boldsymbol{E} + ZeB^2\boldsymbol{\Gamma}_{z,\perp} + \boldsymbol{B}\times\boldsymbol{R}_z. \tag{2.6}$$

This expression contains the flux in both the diamagnetic and radial directions. The flux-surface averaged radial flux becomes

$$\begin{aligned} Ze\left\langle\boldsymbol{\Gamma}_z\cdot\nabla\psi\right\rangle &= \left\langle\frac{\boldsymbol{B}\times\nabla\psi}{B^2}\cdot\boldsymbol{R}_z\right\rangle \\ &+ Ze\left\langle n_z\frac{\boldsymbol{B}\times\nabla\psi}{B^2}\cdot\boldsymbol{E}\right\rangle - \left\langle\frac{\boldsymbol{B}\times\nabla\psi}{B^2}\cdot\nabla p_z\right\rangle, \end{aligned} \tag{2.7}$$

where ψ is an arbitrary flux-surface label and $\langle\cdot\rangle$ denotes the flux-surface average. Here, the first term on the right is the classical flux, and the second one is the radial flux due to the $E\times B$-drift. As there is no radial current in steady-state (i.e. $\nabla\times\boldsymbol{B}\cdot\nabla\psi = 0$), we have

$$\left\langle\boldsymbol{B}\times\nabla\psi\cdot\nabla X\right\rangle = 0 \tag{2.8}$$

for any single-valued function X. The last term of (2.7) can thus be rewritten as $\left\langle p_z\boldsymbol{B}\times\nabla\psi\cdot\nabla B^{-2}\right\rangle$, which is the radial flux due to the magnetic drift of a Maxwellian species. Thus the two latter terms in (2.7) correspond to the neoclassical flux, and will be denoted by $\left\langle\boldsymbol{\Gamma}_z\cdot\nabla\psi\right\rangle^{\mathrm{NC}}$.

From this point, we will assume that the inductive electric field is small, so that $\boldsymbol{E} = -\nabla\Phi$. Following Calvo *et al.* (2018), we obtain a flux-friction relation by introducing two functions, u and w†, defined through the magnetic differential equations

$$\boldsymbol{B}\cdot\nabla u = -\boldsymbol{B}\times\nabla\psi\cdot\nabla B^{-2} \tag{2.9}$$

$$\boldsymbol{B}\cdot\nabla(n_z w) = -\boldsymbol{B}\times\nabla\psi\cdot\nabla(n_z B^{-2}), \tag{2.10}$$

so that

$$\begin{aligned} Ze\left\langle\boldsymbol{\Gamma}_z\cdot\nabla\psi\right\rangle^{\mathrm{NC}} &= \left\langle\boldsymbol{B}\cdot[Zen_z w\nabla\Phi + u\nabla p_z]\right\rangle \\ &= \left\langle\boldsymbol{B}\cdot[(u-w)\nabla p_z + w\boldsymbol{R}_z]\right\rangle, \end{aligned} \tag{2.11}$$

where we have used parallel force-balance to eliminate the parallel electric field from the expression. We can thus evaluate the neoclassical transport for a given n_z, provided that $\left\langle wBR_{z\parallel}\right\rangle$ is known in terms of n_z; such an expression for $R_{z\parallel}$ is presented in Sec. 3. To calculate the friction force, we must however know the parallel impurity flux, which is the subject of the next section.

2.2. *Parallel impurity flux*

From (2.6), we get the impurity flux in the $\boldsymbol{B}\times\nabla\psi$-direction (denoted with a $\wedge$ subscript) as

$$\boldsymbol{\Gamma}_{z\wedge} = \frac{\boldsymbol{B}\times\nabla\psi}{ZeB^2}\left(Zen_z\frac{\partial\Phi}{\partial\psi} + \frac{\partial p_z}{\partial\psi} + \frac{\boldsymbol{R}_z\cdot\nabla\psi}{|\nabla\psi|^2}\right). \tag{2.12}$$

† Note that Calvo *et al.* (2018) defines U_1 instead of w; they are related through $U_1 = wn_z/N_z$.

In a confined plasma, the radial fluxes and thus the radial friction will be small, so we can neglect $\boldsymbol{R}_z \cdot \nabla\psi$ in (2.12) and neglect the radial flux in the impurity continuity equation $\nabla \cdot \boldsymbol{\Gamma}_z = 0$. The parallel impurity flux $\Gamma_{z,\parallel}$ thus satisfies

$$\boldsymbol{B} \cdot \nabla(\Gamma_{z\parallel} B^{-1}) = -\nabla \cdot \boldsymbol{\Gamma}_{z\wedge}. \tag{2.13}$$

In (2.12), the second term will be much smaller when $Z \gg 1$, unless p_z varies on scales Z times shorter than Φ, which is never the case in practice. In the $Z \gg 1$ limit, (2.13) thus becomes (recalling $e\tilde{\Phi}/T \sim Z^{-1}$)

$$\boldsymbol{B} \cdot \nabla(\Gamma_{z\parallel} B^{-1}) = -\frac{\mathrm{d}\langle\Phi\rangle}{\mathrm{d}\psi}\boldsymbol{B} \times \nabla\psi \cdot \nabla\left(\frac{n_z}{B^2}\right) \tag{2.14}$$

so that

$$\Gamma_{z\parallel} \equiv n_z V_{z\parallel} = w n_z \frac{\mathrm{d}\langle\Phi\rangle}{\mathrm{d}\psi} B + B K_z, \tag{2.15}$$

where $K_z(\psi)$ is an integration constant.

3. Parallel friction force

With the parallel impurity flux from the previous section, we now have everything needed to calculate the ion-impurity parallel friction.

As the collisions with electrons can be neglected, the friction force on the impurities can be expressed as

$$\boldsymbol{R}_z \approx \boldsymbol{R}_{zi} = -\boldsymbol{R}_{iz} = -\int \mathrm{d}^3 v m_i \boldsymbol{v} C_{iz}, \tag{3.1}$$

where $\boldsymbol{R}_{ab}$ denotes the friction force on species a by species b, and C_{iz} is the ion-impurity collision operator. Since $m_z \gg m_i$ for high-Z impurities, we can use a mass-ratio expanded ion-impurity collision operator

$$C_{iz} = \nu_{iz}^D(v)\left(\mathcal{L}(f_{i1}) + \frac{m_i \boldsymbol{v} \cdot \boldsymbol{V}_z}{T_i} f_{i0}\right), \tag{3.2}$$

where $\boldsymbol{V}_z = \boldsymbol{\Gamma}_z / n_z$ is the flow of the impurities, $\mathcal{L}$ is the Lorentz operator (Helander & Sigmar 2005), f_{i1} the order ρ_* part of the ion distribution function, and the collision frequency ν_{iz}^D is

$$\nu_{iz}^D = \frac{n_z Z^2 e^4 \ln\Lambda}{4\pi m_i^2 \epsilon_0^2 v^3}. \tag{3.3}$$

The lowest order ion distribution function f_{i0} is taken to be a stationary Maxwell-Boltzmann distribution, and to calculate the parallel friction force we only need the gyrophase-independent part of f_{i1} (which we denote by F_{i1}). This function is given by the ion drift-kinetic equation

$$v_\parallel \nabla_\parallel F_{i1} + \boldsymbol{v}_d \cdot \nabla f_{i0} = C_i, \tag{3.4}$$

where gradients are taken with $\mathcal{E} = mv^2/2 + e\Phi$ and $\mu = m_i v_\perp^2/(2B)$ fixed – although we will later make use of the fact that the potential energy is approximately constant over an ion orbit and use the approximate invariants v and $\lambda = v_\perp^2/(v^2 B)$ as velocity coordinates.

The collision operator is approximately given by collisions with bulk ions and impurities, $C_i \approx C_{iz} + C_{ii}$, and we use a model operator for ion-ion collisions

$$C_{ii} = \nu_{ii}^D(v)\left(\mathcal{L}(F_{i1}) + \frac{m_i \boldsymbol{v} \cdot \boldsymbol{U}}{T_i} f_{i0}\right), \tag{3.5}$$

where $\boldsymbol{U}$ is determined by momentum conservation and the collision frequency is

$$\nu_{ii}^D = \frac{n_i e^4 \ln \Lambda}{4\pi m_i^2 \epsilon_0^2 v^3} \left(\operatorname{erf}\left(v/v_{Ti}\right) - G(v/v_{Ti})\right), \tag{3.6}$$

where erf is the error function and G the Chandrasekhar function (Helander & Sigmar 2005).

We will assume that C_i is smaller than the other terms in (3.4) and expand $F_{i1} = F_{i1}^{(0)} + F_{i1}^{(1)} + \ldots$ in collisionality, so that

$$v_\parallel \nabla_\parallel F_{i1}^{(0)} + \boldsymbol{v}_d \cdot \nabla f_{i0} = 0 \tag{3.7}$$

$$v_\parallel \nabla_\parallel F_{i1}^{(1)} = C_i[F_{i1}^{(0)}]. \tag{3.8}$$

We solve (3.7) and (3.8) as in Newton *et al.* (2017), except that we allow n_z to vary on the flux-surface, which makes the expressions less compact; the details are thus relegated to appendices A–D.

The parallel friction force becomes

$$\begin{aligned} R_{iz,\parallel}\frac{\tau_{iz}}{n_i m_i} = &\left[w - \frac{\langle wB^2\rangle}{\langle B^2\rangle}\right] B\frac{\mathrm{d}\langle\Phi\rangle}{\mathrm{d}\psi} + \left[\frac{1}{n_z} - \frac{\left\langle \frac{B^2}{n_z}\right\rangle}{\langle B^2\rangle}\right] BK_z \\ &- \left[u - \frac{\langle uB^2\rangle}{\langle B^2\rangle}\right] B\frac{T_i}{e}\left[A_{i1} - \frac{3}{2}A_{i2}\right], \end{aligned} \tag{3.9}$$

where $A_{i1} = \frac{\mathrm{d}\ln p_i}{\mathrm{d}\psi} + \frac{e}{T_i}\frac{\mathrm{d}\langle\Phi\rangle}{\mathrm{d}\psi}$ and $A_{2i} = \frac{\mathrm{d}\ln T_i}{\mathrm{d}\psi}$ are the ion thermodynamic forces; $\tau_{iz}^{-1} = Z^2 n_z e^4 \ln\Lambda/(3\pi^{3/2} m_i^2 \epsilon_0^2 v_{Ti}^3)$; K_z is determined by the solvability condition on (2.2), $\langle n_z^{-1} B R_{iz\parallel}\rangle = 0$, and is given by

$$\begin{aligned} K_z(\psi) = &-\left\langle \frac{B^2}{n_z}(1-c_4\alpha)\right\rangle^{-1} \frac{\mathrm{d}\langle\Phi\rangle}{\mathrm{d}\psi}\left\langle (1-c_4\alpha) wB^2\right\rangle \\ &+\left\langle \frac{B^2}{n_z}(1-c_4\alpha)\right\rangle^{-1} \left(c_1 a_2 + b_2 + \left\langle uB^2\right\rangle [c_1+1]\right)\frac{T_i}{e}A_{1i} \\ &+\left\langle \frac{B^2}{n_z}(1-c_4\alpha)\right\rangle^{-1} \left(c_1\left[a_3 - \frac{5}{2}a_2\right] + \left[b_3 - \frac{5}{2}b_2\right] - \left\langle uB^2\right\rangle\left[c_1\eta + \frac{3}{2}\right]\right)\frac{T_i}{e}A_{2i}, \end{aligned} \tag{3.10}$$

where $\alpha = Z^2 n_z/n_i$; $\eta \approx 1.17$; the a_i, b_j and c_k are flux-surface constants which depend on the magnetic geometry and the impurity density variations on the flux-surface, and are defined in equations (C 3)–(C 6), (B 4)–(B 5), and (D 3)–(D 4) in the appendices.

3.1. *Trace impurity limit*

In the trace impurity limit, $\alpha \ll 1$, all the non-standard flux-surface constants – a_i, b_j and c_k – reduce to known functions that only depend on the magnetic geometry, see

(E 1)–(E 6) in Appendix E. The resulting friction force is

$$R_{iz,\parallel}\frac{\tau_{iz}}{n_i m_i} = \left(w - \frac{\langle wB^2\rangle}{n_z\left\langle \frac{B^2}{n_z}\right\rangle}\right) B\frac{\mathrm{d}\langle\Phi\rangle}{\mathrm{d}\psi} \tag{3.11}$$
$$+ \left(\frac{\langle uB^2\rangle}{\langle B^2\rangle} - u + \left(\frac{1}{n_z\left\langle \frac{B^2}{n_z}\right\rangle} - \frac{1}{\langle B^2\rangle}\right)\left[f_s + \langle uB^2\rangle\right]\left[\frac{f_c}{1-f_c}+1\right]\right) B\frac{T_i}{e}A_{i1}$$
$$- \left(\frac{3}{2}\frac{\langle uB^2\rangle}{\langle B^2\rangle} - \frac{3}{2}u + \left(\frac{1}{n_z\left\langle \frac{B^2}{n_z}\right\rangle} - \frac{1}{\langle B^2\rangle}\right)\left[f_s + \langle uB^2\rangle\right]\left[\frac{\eta f_c}{1-f_c}+\frac{3}{2}\right]\right) B\frac{T_i}{e}A_{i2},$$

where f_c and f_s are defined in (E 7) and (E 8). Equation 3.11 can be used to solve for n_z from the parallel momentum equation (2.2), given a mechanism to set $\tilde{\Phi}$. We will not attempt such a daunting task at this time, and instead consider simplifying limits in the following section.

4. $\Delta \ll 1$ limit

In the $\Delta \ll 1$ limit, with $n_z = n_{z0} + n_{z1} + \ldots$, the zeroth-order parallel momentum equation becomes

$$T_z\nabla_\parallel n_{z0} = -Zen_{z0}\nabla_\parallel\Phi, \tag{4.1}$$

so the zeroth order impurity density is given by a Boltzmann response to Φ

$$n_{z0} = N_z(\psi)\mathrm{e}^{-Ze\Phi/T_z}, \tag{4.2}$$

where N_z, sometimes referred to as the *pseudo-density*, is a flux-function. Here, we assume that $\tilde{\Phi}$ is known. This corresponds to $\tilde{\Phi}$ being set by a mechanism unrelated to n_z. This is appropriate in the trace limit, as $Z^2 n_z \ll n_i$ so that Zn_z can be neglected in the quasi-neutrality relation, which would otherwise relate $\tilde{\Phi}$ and n_z.

If (2.5) is used to write Φ in terms of n_{z0}, the first-order parallel momentum equation becomes

$$T_z n_{z0}\nabla_\parallel\left(\frac{n_{z1}}{n_{z0}}\right) = R_{z\parallel}[n_{z0}], \tag{4.3}$$

which has the solvability condition $\left\langle n_{z0}^{-1}BR_{z\parallel}[n_{z0}]\right\rangle = 0$. This is the same solvability condition as that of the exact equation (2.2), except with $n_z \to n_{z0}$, and thus the friction force in (3.11) can be used with $n_z \to n_{z0}$ without introducing any errors that destroy the solvability of (4.3).

From (4.3) and (3.11), n_{z1} can now be obtained numerically for a given Φ or n_{z0}. This is however not required to calculate the flux, as it is enough to know $\nabla_\parallel n_{z1}$ to calculate the radial flux from (2.11), which gives

$$\langle\boldsymbol{\Gamma}_z\cdot\nabla\psi\rangle^{\mathrm{NC}} = \frac{1}{Ze}\left\langle w_0 BR_{z\parallel}\right\rangle, \tag{4.4}$$

where w_0 is given by (2.10) but with $n_z \to n_{z0}$.

Inserting (3.11) into (4.4), the radial flux becomes

$$\frac{\tau_{iz0}n_{z0}}{n_i m_i}\left\langle w_0 B R_{z\parallel}[n_{z0}]\right\rangle = \left(\frac{\left\langle w_0 B^2\right\rangle^2}{\left\langle \frac{B^2}{n_{z0}}\right\rangle} - \left\langle n_{z0} w_0^2 B^2\right\rangle\right)\frac{\mathrm{d}\left\langle \Phi\right\rangle}{\mathrm{d}\psi} \tag{4.5}$$
$$+\left(\left\langle n_{z0} w_0 u B^2\right\rangle - \frac{\left\langle uB^2\right\rangle}{\left\langle B^2\right\rangle}\left\langle n_{z0} w_0 B^2\right\rangle\right)\frac{T_i}{e}\left(A_{i1}-\frac{3}{2}A_{i2}\right)$$
$$+\left(\frac{\left\langle n_{z0} w_0 B^2\right\rangle}{\left\langle B^2\right\rangle} - \frac{\left\langle w_0 B^2\right\rangle}{\left\langle \frac{B^2}{n_{z0}}\right\rangle}\right)\left(f_s + \left\langle uB^2\right\rangle\right)\frac{T_i}{e}\left(\frac{f_c}{1-f_c}\left[A_{1i}-\eta A_{2i}\right] + \left[A_{i1}-\frac{3}{2}A_{i2}\right]\right),$$

which we can decompose into parts driven by density, temperature and potential gradients

$$\left\langle \boldsymbol{\Gamma}_z\cdot\nabla\psi\right\rangle^{\mathrm{NC}} = D_{\Phi}^{\mathrm{NC}}\frac{e}{T_i}\frac{\mathrm{d}\left\langle\Phi\right\rangle}{\mathrm{d}\psi} - D_{n_i}^{\mathrm{NC}}\frac{\mathrm{d}\ln n_i}{\mathrm{d}\psi} - D_{T_i}^{\mathrm{NC}}\frac{\mathrm{d}\ln T_i}{\mathrm{d}\psi}, \tag{4.6}$$

where

$$D_{\Phi}^{\mathrm{NC}} = \frac{n_i m_i}{n_{z0}\tau_{iz0}Ze}\frac{T_i}{e}\left(\frac{\left\langle w_0 B^2\right\rangle^2}{\left\langle \frac{B^2}{n_{z0}}\right\rangle} - \left\langle n_{z0} w_0^2 B^2\right\rangle + \left\langle n_{z0} w_0 u B^2\right\rangle - \frac{\left\langle uB^2\right\rangle}{\left\langle B^2\right\rangle}\left\langle n_{z0} w_0 B^2\right\rangle\right.$$
$$\left. + \left[\frac{\left\langle n_{z0} w_0 B^2\right\rangle}{\left\langle B^2\right\rangle} - \frac{\left\langle w_0 B^2\right\rangle}{\left\langle \frac{B^2}{n_{z0}}\right\rangle}\right]\frac{\left(f_s+\left\langle uB^2\right\rangle\right)}{1-f_c}\right) \tag{4.7}$$

$$D_{n_i}^{\mathrm{NC}} = -\frac{n_i m_i}{n_{z0}\tau_{iz0}Ze}\frac{T_i}{e}\left(\left\langle n_{z0} w_0 u B^2\right\rangle - \frac{\left\langle uB^2\right\rangle}{\left\langle B^2\right\rangle}\left\langle n_{z0} w_0 B^2\right\rangle\right.$$
$$\left. + \left[\frac{\left\langle n_{z0} w_0 B^2\right\rangle}{\left\langle B^2\right\rangle} - \frac{\left\langle w_0 B^2\right\rangle}{\left\langle \frac{B^2}{n_{z0}}\right\rangle}\right]\frac{\left(f_s+\left\langle uB^2\right\rangle\right)}{1-f_c}\right) \tag{4.8}$$

$$D_{T_i}^{\mathrm{NC}} = \frac{1}{2}\frac{n_i m_i}{n_{z0}\tau_{iz0}Ze}\frac{T_i}{e}\left(\left\langle n_{z0} w_0 u B^2\right\rangle - \frac{\left\langle uB^2\right\rangle}{\left\langle B^2\right\rangle}\left\langle n_{z0} w_0 B^2\right\rangle\right. \tag{4.9}$$
$$\left. + \left[\frac{\left\langle n_{z0} w_0 B^2\right\rangle}{\left\langle B^2\right\rangle} - \frac{\left\langle w_0 B^2\right\rangle}{\left\langle \frac{B^2}{n_{z0}}\right\rangle}\right]\frac{\left(f_s+\left\langle uB^2\right\rangle\right)}{1-f_c}\left(1+(2\eta-3)f_c\right)\right)$$

From (4.7), we see that the flux due to the radial electric field is generally non-zero, but that it vanishes when n_{z0} is constant on the surface. The non-zero D_{Φ}^{NC} can in-fact dominate the other neoclassical transport coefficients, as will be seen in Sec. 6

5. Classical transport

Finally, we calculate the classical flux, given by the first term in (2.7). Using our mass-ratio expanded collision operator and momentum conservation, the perpendicular friction becomes

$$\boldsymbol{R}_{zi\perp} = -\int \mathrm{d}^3 v m_i \nu_{iz}^D(v)\left(\boldsymbol{v}_\perp \mathcal{L}(f_{i1}) + \frac{m_i \boldsymbol{v}_\perp \boldsymbol{v}\cdot\boldsymbol{V}_z}{T_i} f_{i0}\right), \tag{5.1}$$

where $\boldsymbol{v}_\perp = \boldsymbol{v} - v_\parallel \boldsymbol{b}$ with $v_\parallel = \boldsymbol{v}\cdot\boldsymbol{b}$.

In (5.1), only the gyrophase-dependent part of f_{i1} contributes to the first term, and

only the perpendicular impurity flow contributes to the last. The gyrophase dependent part of f_{i1} (which we denote $\tilde{f}_{i1}$) is given by Hazeltine (1973)

$$\tilde{f}_{i1} = -\boldsymbol{\rho}_i \cdot \nabla f_{i0}, \tag{5.2}$$

where the gyroradius vector is

$$\boldsymbol{\rho}_i = \rho_i(\boldsymbol{e}_2 \cos\gamma + \boldsymbol{e}_3 \cos\gamma) = \boldsymbol{b} \times \boldsymbol{v}_\perp / \Omega_i, \tag{5.3}$$

with $\{\boldsymbol{b}, \boldsymbol{e}_2, \boldsymbol{e}_3\}$ an orthonormal set of vectors, and $\Omega_i = eB/m_i$. Thus, we have everything required to calculate the perpendicular friction, which becomes

$$\boldsymbol{R}_{zi\perp} = \frac{m_i n_i}{\tau_{iz}} \frac{T_i}{eB} \boldsymbol{b} \times \nabla\psi \left[A_{1i} - \frac{3}{2} A_{2i} \right] - \frac{n_i m_i}{\tau_{iz}} \boldsymbol{V}_{z\perp}. \tag{5.4}$$

Using the same approximations and assumptions as in the neoclassical expressions, we replace $\boldsymbol{V}_{z\perp}$ with $\boldsymbol{v}_E = \boldsymbol{b} \times \nabla\Phi / B$, and thus obtain

$$\boldsymbol{R}_{zi\perp} = \frac{m_i n_i}{n_z \tau_{iz}} n_z \frac{\boldsymbol{B} \times \nabla\psi}{B^2} \frac{T_i}{e} \left[\frac{\mathrm{d}\ln n_i}{\mathrm{d}\psi} - \frac{1}{2} \frac{\mathrm{d}\ln T_i}{\mathrm{d}\psi} \right], \tag{5.5}$$

resulting in the classical impurity flux

$$\begin{aligned} \langle \boldsymbol{\Gamma}_z \cdot \nabla\psi \rangle^{\mathrm{C}} \equiv & \frac{1}{Ze} \left\langle \frac{\boldsymbol{B} \times \nabla\psi}{B^2} \cdot \boldsymbol{R}_z \right\rangle \\ = & \frac{m_i n_i}{Z e n_z \tau_{iz}} \left\langle n_z \frac{|\nabla\psi|^2}{B^2} \right\rangle \frac{T_i}{e} \left[\frac{\mathrm{d}\ln n_i}{\mathrm{d}\psi} - \frac{1}{2} \frac{\mathrm{d}\ln T_i}{\mathrm{d}\psi} \right], \end{aligned} \tag{5.6}$$

or

$$\langle \boldsymbol{\Gamma}_z \cdot \nabla\psi \rangle^{\mathrm{C}} = -D^{\mathrm{C}}_{n_i} \frac{\mathrm{d}\ln n_i}{\mathrm{d}\psi} - D^{\mathrm{C}}_{T_i} \frac{\mathrm{d}\ln T_i}{\mathrm{d}\psi}. \tag{5.7}$$

The classical flux is often neglected as smaller than the neoclassical flux. To get a simple estimate of its importance, we take the homogeneous n_z limit of (4.5) and (5.6), so that the ratio of classical to neoclassical flux depends purely on geometry

$$\frac{\langle \boldsymbol{\Gamma}_z \cdot \nabla\psi \rangle^{\mathrm{C}}}{\langle \boldsymbol{\Gamma}_z \cdot \nabla\psi \rangle^{\mathrm{NC}}} = \frac{\left\langle \frac{|\nabla\psi|^2}{B^2} \right\rangle \langle B^2 \rangle}{\left(\langle u^2 B^2 \rangle \langle B^2 \rangle - \langle u B^2 \rangle^2 \right)}. \tag{5.8}$$

This ratio is indeed small in conventional tokamaks and stellarators (it is ~ 0.1–0.6 in ASDEX Upgrade, and ~ 0.1–1 in LHD), but it is ~ 3–3.5 in a standard W7-X configuration.

W7-X differs from LHD in that it has been optimized to have a low ratio of parallel to perpendicular current. To see how this affects the ratio (5.8), we can express the parallel current in the following way: Charge conservation imposes $\nabla \cdot \boldsymbol{j} = 0$, where $\boldsymbol{j}$ is the current density. Assuming that the equilibrium magnetic field can be written as $\boldsymbol{j} \times \boldsymbol{B} = \nabla p$ – where p is the total pressure $p = \sum_a p_a$, which is assumed to be a flux-function to the required order – the parallel current density becomes $j_\parallel = uB \frac{\mathrm{d}p}{\mathrm{d}\psi}$. The ration of parallel and perpendicular current then becomes

$$\frac{j_\parallel}{|j_\perp|} = \frac{uB}{|\boldsymbol{B} \times \nabla\psi / B^2|}, \tag{5.9}$$

which can be made small by making $u/|\nabla\psi|$ small, which simultaneously makes (5.8) large. The classical flux remains large even when n_z varies on the flux-surface, as we will see in the next section.

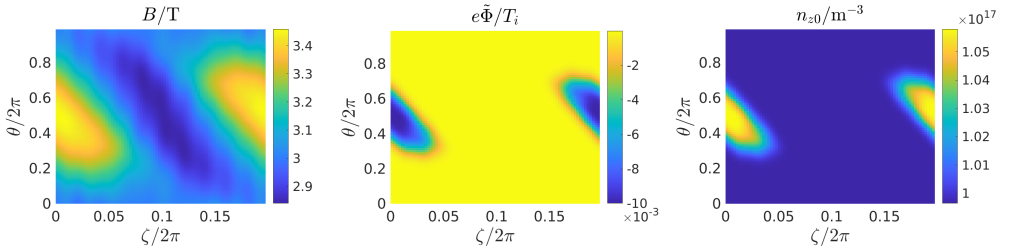

Figure 1: (left) A W7-X standard configuration vacuum field, with (middle) $\tilde{\Phi}$ and (right) n_{z0}, for $\tilde{\Phi}(B) = \tilde{\Phi}(B_0)\mathrm{e}^{-(B-B_0)^2/(2\sigma^2)}$ with $B_0 = B_{\max}$, $\tilde{\Phi}(B_0) = -10\,\mathrm{V}$ and $\sigma = 0.1|B_{\max} - B_{\min}|$, $Z = 6$, $\langle n_z \rangle = 10^{17}\,\mathrm{m}^{-3}$, and $T_i = T_z = 1\,\mathrm{keV}$.

6. Wendelstein 7-X test case

To explore the implications of the flux-surface variation of n_{z0} in (4.7)–(4.9), we consider a scenario where $\tilde{\Phi}$ is given by

$$\tilde{\Phi}(B) = \tilde{\Phi}(B_0)\mathrm{e}^{-(B-B_0)^2/(2\sigma^2)}, \tag{6.1}$$

where $\tilde{\Phi}(B_0)$ is an amplitude of the potential, B_0 is an extremum of B, and σ gives the width of $\tilde{\Phi}$. Equation 6.1 represents a simple case when $\tilde{\Phi}$ is purely a function of B, which is the expected behaviour when $\tilde{\Phi}$ is set by fast particles. Specifically, fast, collisionless particles will have distribution functions that only depend on their constants of motions μ and $\mathcal{E}$. The resulting fast-particle density then only depends on B and Φ,

$$n_\alpha = \int \mathrm{d}^3 v f_\alpha(m_\alpha v_\perp^2/2B, m_\alpha v^2/2 + Z_\alpha e\Phi) = n_\alpha(B, \Phi), \tag{6.2}$$

where the α species subscript denotes a fast-particle species. Assuming that the other species have Boltzmann distributed densities, as in (4.2), quasi-neutrality causes Φ to be a function of B and ψ only.

The size of $e\tilde{\Phi}/T_i$ is roughly given by the ratio of n_α/n_e. Values of $e\tilde{\Phi}/T_i \sim 0.05$ is thus an approximate upper bound; although we are primarily interested in (6.1) as a simple test case, and will not be so concerned with whether it is a realistic fast-particle response.

We take B from a Wendelstein 7-X vacuum field, and solve the magnetic differential equations for u and w numerically for this field. The magnetic field in Boozer coordinates is visualized in Fig. 1, together with an example $\tilde{\Phi}$ and the resulting n_{z0} for $Z = 6$ and $\langle n_{z0} \rangle = 10^{17}\,\mathrm{m}^{-3}$.

To investigate the effects of a localized n_z distribution, we performed a scan where the amplitude of the potential perturbation is increased. Specifically, the potential perturbation is centred at $B_{\max}$ or $B_{\min}$, and the amplitude $\tilde{\Phi}(B_0)$ is scanned from $e\tilde{\Phi}/T_z = -0.1$ to $e\tilde{\Phi}/T_z = 0.1$ – where a negative/positive sign corresponds to impurities accumulating/decumulating at $B_{\max}$. The ion temperature and density are $T_i = 1\,\mathrm{keV}$ and $n_i = 10^{20}\,\mathrm{m}^{-3}$.

The resulting transport coefficients are shown in Fig. 2. In the figures, D (without superscript index) refers to the sum of neoclassical and classical D's; for comparison, we also show D^{NC}. As indicated in Sec. 5, classical transport is dominant for this field configuration, but we also see that the transport due to the radial electric field can be comparable for higher amplitude potential perturbations. We see that both when $B_0 = B_{\max}$ and $B_0 = B_{\min}$, there is a narrow amplitude range, roughly $e\tilde{\Phi}(B_0)/T_i \in [-0.04, 0]$, in which the impurity flux due to an inward radial electric field is weakly

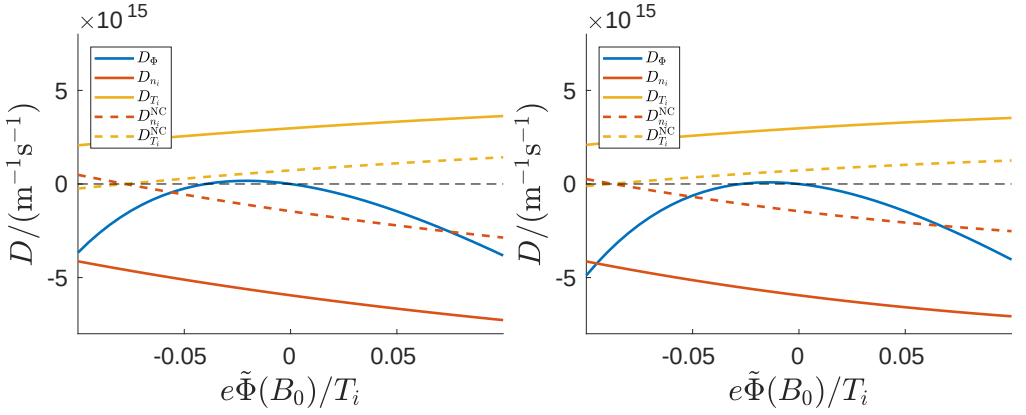

Figure 2: Transport coefficients, for different potential perturbation amplitudes $\tilde{\Phi}(B_0)$, for $\tilde{\Phi}$ localized around (left) $B_{\max}$ and (right) $B_{\min}$. $T_i = 1\,\mathrm{keV}$ and $n_i = 10^{20}\,\mathrm{m}^{-3}$, $\sigma = 0.1|B_{\max} - B_{\min}|$, $Z = 6$, $\langle n_z \rangle = 10^{17}\,\mathrm{m}^{-3}$; D^{NC} refers to the neoclassical transport coefficients, while D is the sum of classical and neoclassical. At amplitudes roughly within $e\tilde{\Phi}/T_i \in [-0.04, 0]$, the flux due to an inward radial electric field is outward but very weak.

positive. Within this window, the flux driven by the electric field is largely unaffected by $\tilde{\Phi}(B_0)$, and the impurities will be driven outwards when the temperature gradient is strong enough, i.e. we have *temperature screening*. Specifically, temperature screening occurs when $\mathrm{d}_\psi \ln T_i \gtrsim 2\mathrm{d}_\psi \ln n_i$, and the magnitude of the flux can be affected by changing the strength of the impurity variation on the flux-surface, but $D_{n_i}/D_{T_i} \approx -2$ to within 1%. At higher potential amplitudes, the radial electric field starts to play a role, but it remains subdominant for realistic amplitudes $e\tilde{\Phi}/T_i \lesssim 0.05$.

From Fig. 2, we also see that most of the variation in D_{n_i} and D_{T_i} comes from the neoclassical flux. This can partly be understood from the simpler form of the classical flux (5.6), where the dependence on n_z is linear, so that the localized n_z perturbation due to $\tilde{\Phi}$ merely acts as a weight in the geometric factor $\langle n_z |\nabla\psi|^2/B^2 \rangle$, which here gives a small effect when integrated over the flux-surface. In contrast, the neoclassical flux (4.5) is non-linear in n_z, and the total flux through the flux-surface is set by a balance between inward and outward fluxes at different points on the flux-surface.

To investigate the effects of more localized fast ions, we scanned the width of $\tilde{\Phi}$, while keeping $\langle \tilde{\Phi} \rangle$ and $\langle n_{z0} \rangle$ constant. For small σ, this results in n_{z0} that are very localized around the extremum of B. The result is shown in Fig. 3. From the figure, we see that D_Φ^{NC} diverges for localized n_{z0}. This is due to the w_0^2 terms in D_Φ^{NC}: $n_{z0}w_0$ obtained from (2.10) is not localized to regions where n_{z0} is localized, which results in a large w_0 where n_{z0} is small. In contrast, the $D_{n_i}^{\mathrm{NC}}$ and $D_{T_i}^{\mathrm{NC}}$ remains finite, as w_0 only appears together with an n_{z0} in those terms. In comparison to the neoclassical transport coefficients, the classical coefficients are only moderately affected by a more localized n_{z0}, for the same reasons as discussed in relation to the amplitude scan above.

To see whether this conclusion holds for more general n_{z0}, we let B_0 in (6.1) be a non-extremum point (within the flux surface), i.e. $B_0 \in (B_{\min}, B_{\max})$. The resulting density distribution n_{z0} will be concentrated or repelled from a contour of B, rather than a point, and do not necessarily represent realistic density variations: rather, they provide simple test cases very different from those considered above, and thus give an indication of how general the above conclusions are.

For $B_0 = B_{\min}/2 + B_{\max}/2$, the resulting D's are displayed in Fig. 4. Here, the D_Φ

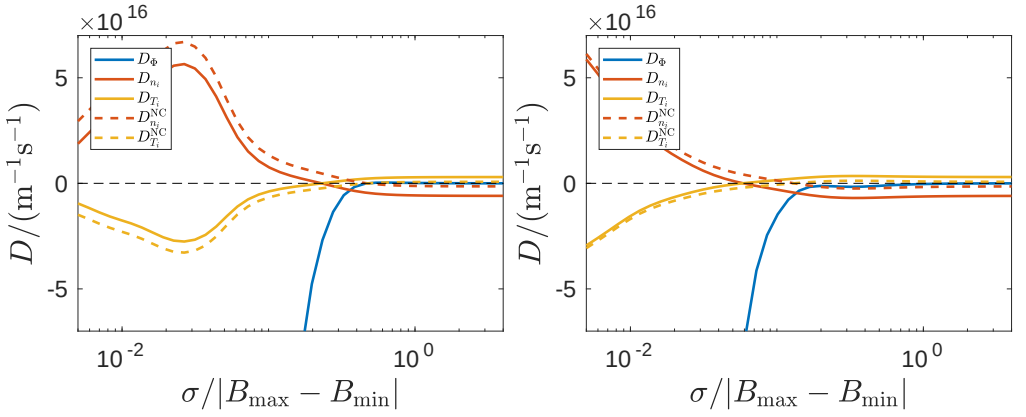

Figure 3: Transport coefficient for varying σ, for $\tilde{\Phi}$ given by (6.1), with $e\left\langle\tilde{\Phi}\right\rangle/T_i = -0.025$ centered around (left) $B_{\max}$, and (right) $B_{\min}$. Unless otherwise stated, quantities have the same value as in Fig. 2

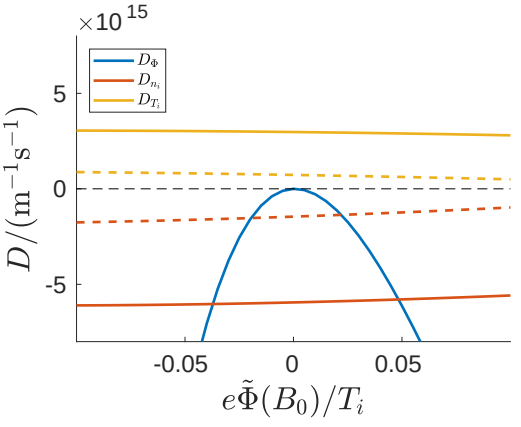

Figure 4: Figure corresponding to Fig. 2, but with n_{z0} concentrated around (or repelled from) the $B = (B_{\min}/2 + B_{\max}/2)$ contour.

increases rapidly with the amplitude, and dominates the flux except for a small interval about 0. Meanwhile, D_{T_i} and D_{n_i} are barely affected, with a slight reduction in magnitude when the impurities are repelled from B_0.

To connect this result to when B_0 is an extremum, we scanned B_0 from $B_{\min}$ to $B_{\max}$. The resulting D's are shown in Fig. 5. Looking at D_Φ, we see that as we go from $B_0 = B_{\min}/2 + B_{\max}/2$ ($x = 0$ in the figure) towards the extrema ($x = 1$ and $x = -1$), D_Φ tends to become less sensitive to the amplitude.

By comparing D_Φ to D_{n_i} or D_{T_i} in Fig. 5, we see that for all B_0, there are no large changes in D_{n_i} or D_{T_i} within the amplitude interval where D_Φ is small enough to not upset temperature screening (this interval is within or slightly outside the dashed lines, which show where $10D_\Phi = D_{n_i} + D_{T_i}$).

To conclude, it thus appears that strong Φ perturbations caused by fast particles are likely to lead to strong impurity accumulation if the radial electric field is pointing inwards, and when the Φ perturbations are weak enough so that the radial electric field

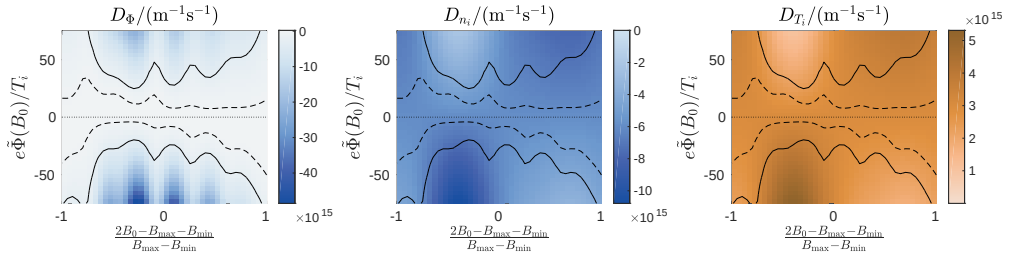

Figure 5: Transport coefficient when B_0 is changed from $B_{\min}$ to $B_{\max}$. Apart from B_0, quantities have the same values as in Fig. 2. The black lines indicate potential amplitudes at which the radial electric field start to dominate: the solid line is where $D_\Phi = D_{n_i} + D_{T_i}$, the dashed is where $10D_\Phi = D_{n_i} + D_{T_i}$.

is not dominant, the condition for temperature screening is essentially unchanged from the $\tilde{\Phi} = 0$ case.

7. Summary & conclusions

We have derived expressions for the radial flux of high-Z collisional impurities when the bulk ions are in the $1/\nu$ regime. In this limit, the impurity temperature is equilibrated with the bulk ions, while the impurity density can vary within the flux-surface. We have derived an expression for the parallel friction-force acting on the impurities, which can be used to solve for the impurity density variations on the flux-surface, given a mechanism for relating the impurity density to the electrostatic potential.

We considered in detail the trace impurity limit, where the electrostatic potential is independent of the impurity density. Using simple models for $\tilde{\Phi}$ and a W7-X vacuum field, we have seen that large $\tilde{\Phi}$ amplitudes can cause the radial electric field to substantially contribute to the impurity transport, and lead to impurity accumulation when the radial electric field points inward. For smaller $\tilde{\Phi}$ amplitudes, temperature screening can be effective, and the condition for temperature screening is essentially the same as in the $\tilde{\Phi} = 0$ case, meaning that the temperature profile should be at least twice as steep as the density profile for screening to happen. In all cases, the contribution from classical transport is substantial, and even moderate $\tilde{\Phi}$ can cause the electric field to dominate if classical transport is not accounted for.

It is however not straightforward to extrapolate from these results to general $\tilde{\Phi}$, as the neoclassical impurity flux does not depend linearly on n_z, so the flux from a general n_z flux-surface distribution is not a superposition of fluxes from simpler n_z distributions. Realistic $\tilde{\Phi}$ or n_z distributions may be needed to evaluate the fluxes accurately, especially when neoclassical transport is comparable to or stronger than the classical. We refer the interested reader to Calvo *et al.* (2018), where an LHD equilibrium with a $\tilde{\Phi}$ set up by particle trapping effects of the bulk ions is considered.

The authors are grateful for the fruitful discussions with the authors of Calvo *et al.* (2018), who considered the same problem independently and in parallel to us, from which we have benefited. This work has been carried out within the framework of the EUROfusion Consortium and has received funding from the Euratom research and training programme 2014-2018 under grant agreement No 633053. The views and opinions expressed herein do not necessarily reflect those of the European Commission. SB and IP were supported by the International Career Grant of Vetenskapsrådet (Dnr. 330-2014-

6313) and IP by Marie Sklodowska Curie Actions, Cofund, Project INCA 600398. SB's visit to Greifswald was supported by Chalmersska forskningsfonden.

Appendix A. Solving the ion drift-kinetic equation

In this section, we solve (3.7) for $F_{i1}^{(0)}$. The solution follows Newton *et al.* (2017), but here n_z is allowed to vary on the flux-surface. Since we assume $e\tilde{\Phi}/T_i \sim Z^{-1}$, the potential energy of the bulk ions is approximately constant on the flux-surface, and we change variables from $\mathcal{E}$, μ to the approximate invariants v and λ.

Equation 3.7 can be formally solved by integrating along a field-line; using l to denote the distance along the field line, we have

$$F_{i1}^{(0)}(l) = F_{i1}^{(0)}(l_0) - \int_{l_0}^{l} \frac{dl'}{v_\parallel} \boldsymbol{v}_d \cdot \nabla f_{i0}(l'), \tag{A 1}$$

where l_0 is an arbitrary point along the field line and the integration constant $F_{i1}^{(0)}(l_0)$ is set by the solvability condition of the first-order equation. As only the parts of $F_{i1}^{(0)}(l_0)$ that are odd in $v_\parallel$ will contribute to the parallel friction force, it is convenient to take l_0 as a bounce-point, $B(l_0) = 1/\lambda$, which sets the odd part of $F_{i1}^{(0)}(l_0)$ to zero in the trapped region.

In the passing region, $F_{i1}^{(0)}$ is set by

$$\left\langle \frac{B}{v_\parallel} C_i[F_{i1}^{(0)}] \right\rangle = 0. \tag{A 2}$$

Using $\mathcal{L} = \frac{2v_\parallel}{v^2 B} \frac{\partial}{\partial \lambda} \lambda v_\parallel \frac{\partial}{\partial \lambda}$, and integrating once with respect to λ, (A 2) becomes

$$\begin{aligned} &\frac{\partial}{\partial \lambda} F_{i1}^{(0)}(l_0) \qquad\qquad (A\,3)\\ &= -\frac{mv^2}{2\left\langle \left[1 + \frac{\nu_{iz}^D(l)}{\nu_{ii}^D}\right] v_\parallel \right\rangle} \left(\frac{1}{e} \left\langle \left[1 + \frac{\nu_{iz}^D(l)}{\nu_{ii}^D}\right] g_4(l,\lambda) \right\rangle \frac{\partial f_{i0}}{\partial \psi} + \frac{1}{T_i} f_{i0} \left\langle B \left[U_\parallel + \frac{\nu_{iz}^D(l)}{\nu_{ii}^D} V_{z\parallel} \right] \right\rangle \right) \end{aligned}$$

in the passing region. To account for the $\boldsymbol{v}_d \cdot \nabla f_{i0}$ term, we have introduced the geometric function (Nakajima *et al.* 1989)

$$g_4(\lambda, l) = v_\parallel \int_{l_0}^{l} \mathrm{d}l' \, (\boldsymbol{b} \times \nabla \psi) \cdot \nabla \left(\frac{1}{v_\parallel} \right). \tag{A 4}$$

Appendix B. Parallel friction force

Once $U_\parallel$ and $V_{z\parallel}$ are known, we can use (A 3) to directly evaluate the parallel friction force acting on the impurities. From our mass-ratio expanded ion-impurity collision operator (3.2) and the self-adjointness of the Lorentz operator, we have

$$\begin{aligned} R_{iz\parallel} =& \int \mathrm{d}^3 v m_i v_\parallel \nu_{iz}^D(v) \left(\frac{m_i v_\parallel \cdot V_{z\parallel}}{T_i} f_{i0} - F_{i1} \right) \\ =& \frac{n_i m_i}{\tau_{iz}} \left(V_{z\parallel} - \frac{T_i}{e} \left[A_{i1} - \frac{3}{2} A_{i2} \right] Bu - BP(\psi) \right), \end{aligned} \tag{B 1}$$

where P is a flux-function which contains the contribution from the integration constant $F_{i1}^{(0)}(l_0)$

$$P(\psi) \equiv \frac{\tau_{iz}}{Bn_i} \int \mathrm{d}^3 v v_\parallel \nu_{iz}^D(v) F_{i1}^{(0)}(l_0). \tag{B 2}$$

$P(\psi)$ can be evaluated using (A 3) and partial integration in λ

$$P(\psi) = \frac{\langle BU_\parallel \rangle}{\langle B^2 \rangle} b_1 + \frac{\langle \alpha B V_{z\parallel} \rangle}{\langle B^2 \rangle} b_4 + \frac{T_i}{e} \frac{A_{1i} - \frac{5}{2} A_{2i}}{\langle B^2 \rangle} b_2 + \frac{T_i}{e} \frac{A_{2i}}{\langle B^2 \rangle} b_3 \tag{B 3}$$

where we have introduced

$$b_1 = \frac{m\pi \langle B^2 \rangle}{n_i T_i \{\nu_D^{iz}\}} \int_0^\infty \mathrm{d}v v^4 \nu_D^{iz} f_{i0} \int_0^{1/B_{\max}} \mathrm{d}\lambda\, \lambda \frac{1}{\langle \xi \rangle + \left\langle \frac{\nu_{iz}^D}{\nu_{ii}^D} \xi \right\rangle} \tag{B 4}$$

$$b_2 = \frac{m\pi \langle B^2 \rangle}{n_i T_i \{\nu_D^{iz}\}} \int_0^\infty \mathrm{d}v v^4 \nu_D^{iz} f_{i0} \int_0^{1/B_{\max}} \mathrm{d}\lambda\, \lambda \frac{\left[\langle g_4 \rangle + \left\langle \frac{\nu_{iz}^D}{\nu_{ii}^D} g_4 \right\rangle \right]}{\langle \xi \rangle + \left\langle \frac{\nu_{iz}^D}{\nu_{ii}^D} \xi \right\rangle} \tag{B 5}$$

$$b_3 = \frac{m\pi \langle B^2 \rangle}{n_i T_i \{\nu_D^{iz}\}} \int_0^\infty \mathrm{d}v v^4 \frac{m_i v^2}{2T_i} \nu_D^{iz} f_{i0} \int_0^{1/B_{\max}} \mathrm{d}\lambda\, \lambda \frac{\left[\langle g_4 \rangle + \left\langle \frac{\nu_{iz}^D}{\nu_{ii}^D} g_4 \right\rangle \right]}{\langle \xi \rangle + \left\langle \frac{\nu_{iz}^D}{\nu_{ii}^D} \xi \right\rangle} \tag{B 6}$$

$$b_4 = \frac{m\pi \langle B^2 \rangle}{Z^2 n_z T_i \{\nu_D^{iz}\}} \int_0^\infty \mathrm{d}v v^4 \nu_D^{iz} \frac{\nu_D^{iz}}{\nu_{ii}^D} f_{i0} \int_0^{1/B_{\max}} \mathrm{d}\lambda\, \lambda \frac{1}{\langle \xi \rangle + \left\langle \frac{\nu_{iz}^D}{\nu_{ii}^D} \xi \right\rangle}, \tag{B 7}$$

with $\xi = \boldsymbol{v} \cdot \boldsymbol{b}/v$. The velocity average $\{\cdot\}$ is defined as

$$\{F(v)\} \equiv \frac{8}{3\sqrt{\pi}} \int_0^\infty \mathrm{d}x\, F(x) x^4 e^{-x^2}, \tag{B 8}$$

where $x = v/v_{Ti}$.

To have the boundary terms from the partial integration disappear in (B 3), we have defined l_0 through $B(l_0) = B_{\max}$. This makes our choice of l_0 continuous when going from the trapped to the passing region, and thus ensures that $F_{i1}^{(0)}(l_0)$ is zero at the trapped-passing boundary $\lambda = 1/B_{\max}$.

Appendix C. Momentum restoring term $U_\parallel$

The momentum restoring term in the ion-ion model collision operator (3.5) is calculated so that ion-ion collisions conserve momentum. Specifically, we have

$$U_\parallel = \frac{1}{n_i \{\nu_D^{ii}\}} \int \mathrm{d}^3 v v_\parallel \nu_D^{ii} F_{i1}^{(0)}. \tag{C 1}$$

Inserting $F_{i1}^{(0)}$ from (A 1) and using (A 3), we get

$$\begin{aligned} &\langle BU_\parallel \rangle (1 - a_1) \\ =&\frac{T_i}{e} \left(\left[a_2 + \langle uB^2 \rangle \right] A_{1i} + \left[a_3 - \frac{5}{2} a_2 - \langle uB^2 \rangle \eta \right] A_{2i} \right) + a_4 \langle \alpha B V_{z\parallel} \rangle . \end{aligned} \tag{C 2}$$

where we have defined the geometry-impurity dependent flux-surface constants

$$a_1 = \frac{m\pi\left\langle B^2\right\rangle}{n_i T_i\{\nu_D^{ii}\}}\int_0^\infty \mathrm{d}v v^4 \nu_D^{ii} f_{i0}\int_0^{1/B_{\max}} \mathrm{d}\lambda\,\lambda \frac{1}{\langle\xi\rangle + \left\langle \frac{\nu_{iz}^D}{\nu_{ii}^D}\xi\right\rangle} \tag{C 3}$$

$$a_2 = \frac{m\pi\left\langle B^2\right\rangle}{n_i T_i\{\nu_D^{ii}\}}\int_0^\infty \mathrm{d}v v^4 \nu_D^{ii} f_{i0}\int_0^{1/B_{\max}} \mathrm{d}\lambda\,\lambda \frac{\left[\langle g_4\rangle + \left\langle \frac{\nu_{iz}^D}{\nu_{ii}^D} g_4\right\rangle\right]}{\langle\xi\rangle + \left\langle \frac{\nu_{iz}^D}{\nu_{ii}^D}\xi\right\rangle} \tag{C 4}$$

$$a_3 = \frac{m\pi\left\langle B^2\right\rangle}{n_i T_i\{\nu_D^{ii}\}}\int_0^\infty \mathrm{d}v v^4 \frac{m_i v^2}{2T_i} \nu_D^{ii} f_{i0}\int_0^{1/B_{\max}} \mathrm{d}\lambda\,\lambda \frac{\left[\langle g_4\rangle + \left\langle \frac{\nu_{iz}^D}{\nu_{ii}^D} g_4\right\rangle\right]}{\langle\xi\rangle + \left\langle \frac{\nu_{iz}^D}{\nu_{ii}^D}\xi\right\rangle} \tag{C 5}$$

$$a_4 = \frac{m\pi\left\langle B^2\right\rangle}{Z^2 n_z T_i\{\nu_D^{ii}\}}\int_0^\infty \mathrm{d}v v^4 \nu_{iz}^D f_{i0}\int_0^{1/B_{\max}} \mathrm{d}\lambda\,\lambda \frac{1}{\langle\xi\rangle + \left\langle \frac{\nu_{iz}^D}{\nu_{ii}^D}\xi\right\rangle} \tag{C 6}$$

and the boundary condition for u is $u(l_0) = 0$.

Appendix D. Solvability condition and K_z

From (2.15), $V_{z\parallel}$ is known up to a flux-function K_z. The solvability condition of (2.2) states that

$$\left\langle \frac{BR_{z\parallel}}{n_z}\right\rangle = 0, \tag{D 1}$$

which we use to determine K_z. Inserting (B 1), the solvability condition becomes

$$\frac{n_i m_i}{n_z \tau_{iz}}\left(\left\langle BV_{z\parallel}\right\rangle - \frac{T_i}{e}\left[A_{i1} - \frac{3}{2}A_{i2}\right]\left\langle uB^2\right\rangle - \left\langle B^2\right\rangle P(\psi)\right) = 0. \tag{D 2}$$

For the sake of compactness, we also define

$$c_1 = b_1/(1 - a_1), \tag{D 3}$$

$$c_4 = b_4 + a_4 c_1; \tag{D 4}$$

this results in (3.10).

Appendix E. Trace impurity limit of some expressions

In the trace impurity limit, $\alpha \equiv Z^2 n_z/n_i \ll 1$, the a_i, b_j and c_k's simplify considerably, yielding an expression for K_z in terms of standard geometry functions. Specifically,

$$a_1 = b_1 = f_c, \tag{E 1}$$

$$a_2 = b_2 = f_s, \tag{E 2}$$

$$a_3 = f_s\left(\frac{5}{2} - \eta\right), \tag{E 3}$$

$$b_3 = f_s, \tag{E 4}$$

$$a_4 = \frac{f_c}{\alpha}\frac{\{\nu_D^{iz}\}}{\{\nu_D^{ii}\}}, \tag{E 5}$$

$$b_4 = \frac{f_c}{\alpha}\frac{\{{\nu_D^{iz}}^2/\nu_D^{ii}\}}{\{\nu_D^{iz}\}}. \tag{E 6}$$

Note that a_4 and b_4 only appear in terms containing α, which are negligible in the trace-limit. Here,

$$f_c = \frac{3\left\langle B^2\right\rangle}{4}\int_0^{1/B_{\max}} \mathrm{d}\lambda \frac{\lambda}{\langle\xi\rangle} \tag{E 7}$$

$$f_s = \frac{3\left\langle B^2\right\rangle}{4}\int_0^{1/B_{\max}} \mathrm{d}\lambda \frac{\lambda\left\langle g_4\right\rangle}{\langle\xi\rangle}, \tag{E 8}$$

are standard functions of geometry. With this, K_z becomes

$$\begin{aligned} &K_z(\psi)\left\langle\frac{B^2}{n_z}\right\rangle \\ =&\frac{T_i}{e}\left[f_s + \left\langle uB^2\right\rangle\right]\left(\left[\frac{f_c}{1-f_c}+1\right]A_{1i} - \left[\frac{\eta f_c}{1-f_c}+\frac{3}{2}\right]A_{2i}\right) - \frac{\mathrm{d}\left\langle\Phi\right\rangle}{\mathrm{d}\psi}\left\langle wB^2\right\rangle. \end{aligned} \tag{E 9}$$

REFERENCES

Angioni, C. & Helander, P. 2014 Neoclassical transport of heavy impurities with poloidally asymmetric density distribution in tokamaks. *Plasma Physics and Controlled Fusion* **56** (12), 124001.

Angioni, C., Mantica, P., Pütterich, T., Valisa, M., Baruzzo, M., Belli, E., Belo, P., Casson, F., Challis, C., Drewelow, P., Giroud, C., Hawkes, N., Hender, T., Hobirk, J., Koskela, T., Taroni, L. L., Maggi, C., Mlynar, J., Odstrcil, T., Reinke, M., Romanelli, M. & JET EFDA Contributors 2014 Tungsten transport in JET H-mode plasmas in hybrid scenario, experimental observations and modelling. *Nuclear Fusion* **54** (8), 083028.

Braun, S. & Helander, P. 2010 Pfirsch-Schlüter impurity transport in stellarators. *Physics of Plasmas* **17** (7), 072514.

Calvo, I., Parra, F. I., Velasco, J. L., Alonso, J. A. & García-Regaña, J. M. 2018 Stellarator impurity flux driven by electric fields tangent to magnetic surfaces. *ArXiv e-prints* .

Fülöp, T. & Helander, P. 1999 Nonlinear neoclassical transport in a rotating impure plasma with large gradients. *Physics of Plasmas* **6** (8), 3066–3075.

García-Regaña, J., Beidler, C., Kleiber, R., Helander, P., Mollén, A., Alonso, J., Landreman, M., Maassberg, H., Smith, H., Turkin, Y. & Velasco, J. 2017 Electrostatic potential variation on the flux surface and its impact on impurity transport. *Nuclear Fusion* **57** (5), 056004.

Hazeltine, R. D. 1973 Recursive derivation of drift-kinetic equation. *Plasma Physics* **15** (1), 77.

Helander, P. 1998 Bifurcated neoclassical particle transport. *Physics of Plasmas* **5** (11), 3999–4004.

Helander, P., Newton, S. L., Mollén, A. & Smith, H. M. 2017 Impurity transport in a mixed-collisionality stellarator plasma. *Phys. Rev. Lett.* **118**, 155002.

Helander, P. & Sigmar, D. 2005 *Collisional Transport in Magnetized Plasmas*. Cambridge University Press.

Hirsch, M., Baldzuhn, J., Beidler, C., Brakel, R., Burhenn, R., Dinklage, A., Ehmler, H., Endler, M., Erckmann, V., Feng, Y., Geiger, J., Giannone, L., Grieger, G., Grigull, P., Hartfuss, H.-J., Hartmann, D., Jaenicke, R., König, R., Laqua, H. P., Maassberg, H., McCormick, K., Sardei, F., Speth, E., Stroth, U., Wagner, F., Weller, A., Werner, A., Wobig, H., Zoletnik, S. & the W7-AS Team 2008 Major results from the stellarator Wendelstein 7-AS. *Plasma Physics and Controlled Fusion* **50** (5), 053001.

Kazakov, Y. O., Pusztai, I., Fülöp, T. & Johnson, T. 2012 Poloidal asymmetries due to ion cyclotron resonance heating. *Plasma Physics and Controlled Fusion* **54** (10), 105010.

Mollén, A., Landreman, M., Smith, H. M., García-Regaña, J. M. & Nunami, M.

2018 Flux-surface variations of the electrostatic potential in stellarators: Impact on the radial electric field and neoclassical impurity transport. Submitted to *Plasma Physics and Controlled Fusion*.

Mollén, A., Pusztai, I., Fülöp, T., Kazakov, Y. O. & Moradi, S. 2012 Effect of poloidal asymmetries on impurity peaking in tokamaks. *Physics of Plasmas* **19** (5), 052307.

Mollén, A., Pusztai, I., Reinke, M. L., Kazakov, Y. O., Howard, N. T., Belli, E. A., Fülöp, T. & The Alcator C-Mod Team 2014 Impurity transport in Alcator C-Mod in the presence of poloidal density variation induced by ion cyclotron resonance heating. *Plasma Physics and Controlled Fusion* **56** (12), 124005.

Nakajima, N., Okamoto, M., Todoroki, J., Nakamura, Y. & Wakatani, M. 1989 Optimization of the bootstrap current in a large helical system with L = 2. *Nuclear Fusion* **29** (4), 605–616.

Newton, S. L., Helander, P., Mollén, A. & Smith, H. M. 2017 Impurity transport and bulk ion flow in a mixed collisionality stellarator plasma. *Journal of Plasma Physics* **83** (5), 905830505.

Rutherford, P. H. 1974 Impurity transport in the pfirschschlter regime. *The Physics of Fluids* **17** (9), 1782–1784.